How to cite: *Angew. Chem. Int. Ed.* **2023**, *62*, e202308408
doi.org/10.1002/anie.202308408

Protein Recognition

Display Selection of a Hybrid Foldamer–Peptide Macrocycle

Sebastian Dengler[+], Ryan T. Howard[+], Vasily Morozov[+], Christos Tsiamantas[+], Wei-En Huang, Zhiwei Liu, Christopher Dobrzanski, Vojislava Pophristic, Sophie Brameyer, Céline Douat, Hiroaki Suga, and Ivan Huc**

Abstract: Expanding the chemical diversity of peptide macrocycle libraries for display selection is desirable to improve their potential to bind biomolecular targets. We now have implemented a considerable expansion through a large aromatic helical foldamer inclusion. A foldamer was first identified that undergoes flexizyme-mediated tRNA acylation and that is capable of initiating ribosomal translation with yields sufficiently high to perform an mRNA display selection of macrocyclic foldamer–peptide hybrids. A hybrid macrocyclic nanomolar binder to the C-lobe of the E6AP HECT domain was selected that showed a highly converged peptide sequence. A crystal structure and molecular dynamics simulations revealed that both the peptide and foldamer are helical in an intriguing reciprocal stapling fashion. The strong residue convergence could be rationalized based on their involvement in specific interactions with the target protein. The foldamer stabilizes the peptide helix through stapling and through contacts with key residues. These results altogether represent a significant extension of the chemical space amenable to display selection and highlight possible benefits of inserting an aromatic foldamer into a peptide macrocycle for the purpose of protein recognition.

Peptide and protein display technologies based on nucleic acid sequence encoding are a powerful way to identify potent and selective ligands for biomolecular targets. Such technologies have demonstrated their clinical potential in the development of a range of approved antibody therapies from phage display platforms,[1] and the discovery of peptidic drugs such as ecallantide[2] and romiplostim.[3] Many modern display technologies leverage the incorporation of non-natural modifications into peptide libraries to expand the chemical diversity of these molecules beyond the natural catalogue[4] and allow the discovery of peptides with desirable pharmacological profiles, including resistance to proteolytic degradation, cell permeability, and novel modes of binding.[5] Incorporation of these non-natural modifications, for example, for the purpose of macrocyclization, has been achieved through either post-translational modification,[6] exploitation of the promiscuity of the ribosome,[7] or genetic engineering of library host organisms.[8]

The remarkable tolerance of the ribosome to accept amino acids with abiotic modifications has recently been highlighted by the incorporation of aromatic oligoamide foldamers (AOFs) into the nascent peptide chain (Figure 1a, b). Pyridine (P) and quinoline (Q) containing oligomers were charged onto tRNA by flexizymes and ribosomally incorporated into the polypeptide chain, affording AOF–peptide hybrids with up to five P/Q-units as translation initiators,[9] or up to three P/Q-units as side-chain appendages.[10] Functionalization of the N-terminus as a chloroacetamide also allowed for spontaneous macrocyclization with a downstream cysteine thiol.[9a,10] The main interest of introducing AOF segments within a peptide macrocycle lies in their inherent folding information. The propensity of Q_n and $(PQ)_n$ oligomers to adopt stable helical conformations is well-documented.[11] Within a hybrid macrocycle, folding of the helical aromatic segment prevails and alters the peptide conformation, for example by stretching the peptide backbone.[9a,12] It also confers resistance towards proteolytic degradation of the peptide.[12] In addition, AOFs themselves have potential for directly interacting with proteins[13] and they exist as natural products.[14] It was

[*] Dr. S. Dengler,[+] Dr. R. T. Howard,[+] Dr. V. Morozov,[+] C. Douat, Prof. I. Huc
Department of Pharmacy and Center for Integrated Protein Science, Ludwig-Maximilians-Universität
Butenandtstr. 5–13, 81377 München (Germany)
E-mail: ivan.huc@cup.lmu.de

Dr. C. Tsiamantas,[+] W.-E. Huang, Prof. H. Suga
Department of Chemistry, School of Science, The University of Tokyo
7-3-1 Hongo, Bunkyo, 113-0033 Tokyo (Japan)
E-mail: hsuga@chem.s.u-tokyo.ac.jp

Prof. Z. Liu, Dr. C. Dobrzanski, Prof. V. Pophristic
Department of Chemistry & Biochemistry, Rowan University
201 Mullica Hill Road, 08028 Glassboro, New Jersey (USA)

Dr. S. Brameyer
Biozentrum, Microbiology, Ludwig-Maximilians-Universität
Großhaderner Str. 2–4, 82152 Martinsried (Germany)

[+] These authors contributed equally to this work.

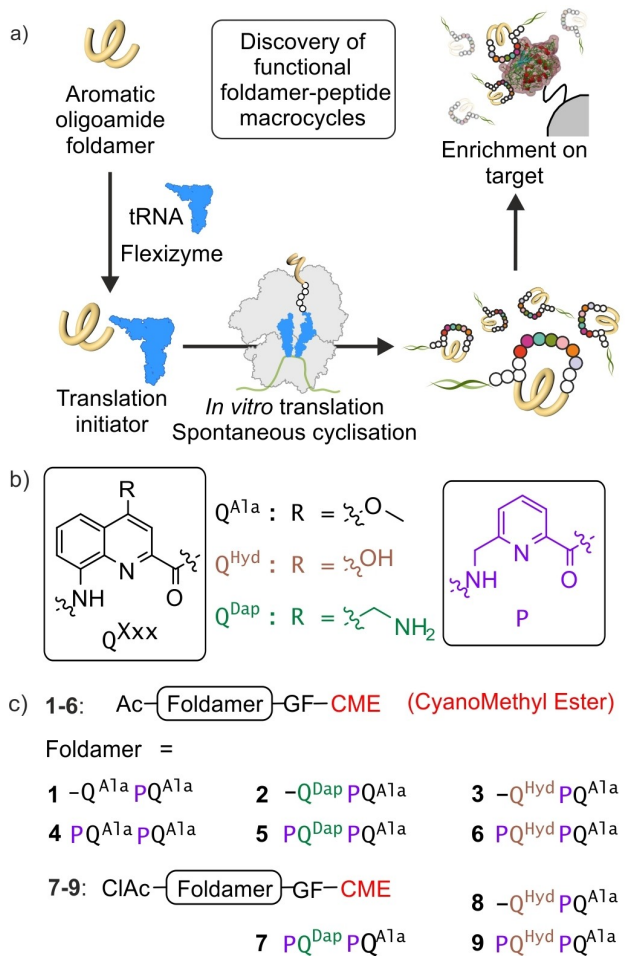

Figure 1. a) Incorporation of aromatic oligoamide foldamers by the flexible in vitro translation (FIT) system into macrocyclic peptide–foldamer hybrids that can undergo selection against a molecular target by mRNA display. b) Nomenclature of the quinoline/pyridine foldamer units used in this study. c) Aromatic foldamer substrates tested for their suitability as translation initiators.

therefore a logical next step to challenge ribosomal translation not just with the production of one AOF–peptide macrocycle, but with an entire DNA-encoded library of such macrocycles.

Herein we show that FIT-synthesized macrocyclic AOF–peptide hybrids are compatible with mRNA display selection using the random nonstandard peptides integrated discovery (RaPID) platform. Translation initiators containing the foldamer element were optimized for tRNA acylation and translation efficiency, and one initiator was successfully utilized in a selection experiment, generating the first biologically evolved AOF–peptide hybrid macrocycle against a protein target, the catalytic C-lobe of the E6AP HECT domain (Figure S4).[15] This E3 ligase was chosen as a proof-of-concept bait protein given its use in a previously successful peptide affinity selection campaign with the RaPID platform.[16] A crystal structure of the macrocycle–protein complex revealed that both the peptide and foldamer are helical in an intriguing reciprocal stapling fashion.

We first set out to identify a foldamer giving sufficiently high yields of both flexizyme-mediated tRNA acylation and ribosomal peptide initiation for the purpose of display selection. N-acylated P/Q-based helical oligoamides **1–6** were prepared (Figure 1b, c). The P units serve to introduce some flexibility,[9a,17] and side chains on Q units were selected to be either cationic (Q^{Dap}), neutral (Q^{Ala}), or anionic (Q^{Hyd}),[18] though all were kept small to reduce possible steric hindrance in the ribosome exit tunnel. The terminal Phe cyanomethyl ester serves as a substrate for the flexizyme. Acylation was assessed using a tRNA mimic, microhelix RNA (mhRNA), demonstrating acylation efficiencies ranging from 0 to 85 % (Table 1, Figure S1). Initiator-charged $tRNA^{fMet}$ molecules, that is, Ac-foldamer-GF-$tRNA^{fMet}$(CAU), were prepared and each was supplemented into a Met-deficient in vitro translation system along with an mRNA template. Expression of the desired foldamer–peptide hybrids was demonstrated by MALDI-TOF-MS and quantified using autoradiographic gel electrophoresis (Table 1, Figures S2 and S3).

These experiments allowed for the identification of top performers **3**, **5** and **6**. Oligoamides **7–9** were then prepared as N-chloroacetylated (ClAc) analogues of **3**, **5** and **6**. tRNA acylation and expression efficiency—including cyclization with a downstream Cys—were determined again (Table 1). The results led to the selection of **7**, which showed the highest expression efficiency, as an initiator for display selection experiments (Figure 2a, b).[19]

Two independent RaPID selections were carried out from NNK (N = A/C/G/T, K = G/T) libraries having randomized windows of either 4–9 or 10–15 peptide residues, all including a mandatory Cys and using **7** as the initiator (Figure 2c). We surmised that the PQPQ segment would have a larger effect on the structure of shorter peptides,[9a,12] but did not know whether this would represent a selection advantage. After five rounds of in vitro selection and amplification, a clear increase in the number of peptides selectively captured by magnetic beads-immobilized C-lobe was observed for both libraries (Figure 2d, left, Figure S5), suggesting the emergence of selective binders. Next-generation sequencing of the recovered DNA libraries hinted at

Table 1: Yields of tRNA acylation and peptide translation with foldamer initiators.

Initiator	N-terminus	Acylation [%]	Translation[a] [%]
1	Ac	0	–
2	Ac	16	5
3	Ac	75	12
4	Ac	14	*N/D*[b]
5	Ac	55	12
6	Ac	85	13
7	ClAc	38	8[c]
8	ClAc	35	2[c]
9	ClAc	67	6[c]

[a] Relative to the same reaction with canonical amino acids only (no reprogramming). [b] Smearing did not allow accurate quantification. [c] The template used for quantification is different from that used for other entries.

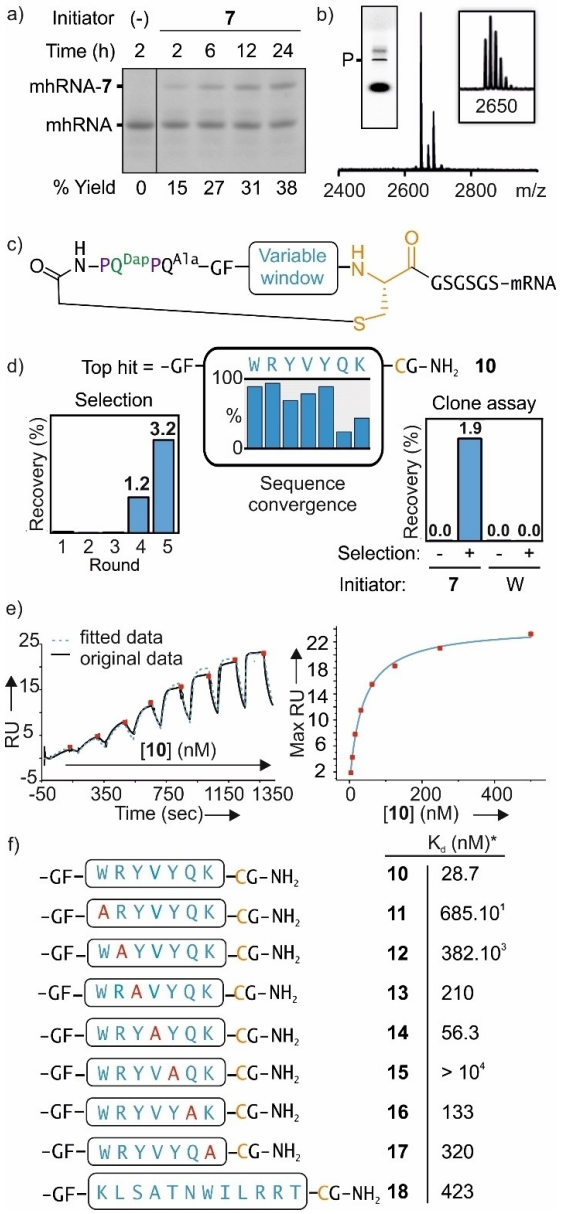

Figure 2. a) Flexizyme-assisted loading of **7** onto truncated tRNA (mhRNA) assessed by PAGE; yields were determined by band intensity ratio (mhRNA-**7** vs. unmodified mhRNA). b) MALDI MS spectrum of a successfully translated peptide–foldamer macrocycle (see Supporting Information for sequence). The three peaks are the H^+, Na^+ and K^+ adducts; right inset = zoom; left inset = quantification of translation (P, 8% yield relative to a standard) by radioisotope incorporation. c) General structure of the library of macrocycle–mRNA conjugates. d) Most enriched sequence from the library of smaller macrocycles; sequence conservation after alignment of the top 20 hits is shown; left inset = recovery of DNA after each round of selection as compared to the input library; right inset = recovery of DNA when RaPID selection was performed once with the clonal mRNA of the top hit, using **7** or ClAc-Trp-CME (W) as the initiator, against blank beads (−) or C-lobe modified beads (+); e) SPR sensorgrams (left) of **10** against C-lobe immobilized on CM5 chips and saturation curve (right) of **10** binding to C-lobe. The steady-state data points are also indicated as red squares on the sensorgrams. Both kinetic and steady-state data fit to a 1:1 binding model (blue lines). f) Peptide segments of **10**–**18** having the formula shown in c) and K_d values of their complex with C-lobe determined by SPR. Boxes indicate variable windows.

an influence of the abiotic segment. The short library converged to a practically unique sequence with a randomized region of seven amino acid residues (Figure 2d, middle, Figure S6). With the longer library, no such convergence was observed (Figure S6). To assess selectivity for C-lobe and the necessity of the foldamer segment, we conducted independent rounds of selection with only the top mRNA sequence of each library. Challenging the translation products of these sequences against beads with and without C-lobe (so-called clone assay) resulted in the binding and recovery of material only when C-lobe was present, suggesting binding of these sequences to the target (Figure 2d right, Figure S7). When the experiment was conducted by substituting the ClAc-foldamer-GF-tRNA^{fMet} initiator with ClAc-Trp-tRNA^{fMet}, binding of the shorter peptide macrocycle was abolished, highlighting a direct or indirect, but essential role of the foldamer in the binding interactions. The effect was lower in the case of the peptide from the larger macrocycle library. Given these results, further studies focused on a hit from the enriched species of the smaller macrocycle library.

Foldamer–peptide macrocycles **10** and **18** (Figure 2d), analogues of the top hits from both library NNK4–9 and library NNK10–15, were then chemically synthesized, first by automated solid-phase synthesis of the peptide segment, followed by automated solid-phase foldamer synthesis to install the PQ^{Dap}PQ^{Ala} tetramer. Subsequent manual incorporation of the N-terminal chloroacetamide was performed on-resin before cleavage and side chain deprotection, thioether macrocyclization, and purification by reverse-phase HPLC. As shown in Figure 2e and 2f, the binding of **10** to C-lobe was demonstrated by surface plasmon resonance (SPR), with C-lobe immobilized on the SPR chip. A K_d of 29 nM was extracted from curve fitting of the sensorgrams with a 1:1 binding isotherm (Figure 2e, f). The K_d value of **18** is over fourteen times larger and this compound was not investigated further (See Figure S8 for the sensorgrams). In contrast with the above, when C-lobe was not immobilized, attempts to measure K_d values using ITC or fluorescence anisotropy with a fluorescein-labelled derivative of **10** were hampered by protein aggregation. C-lobe solutions were notably viscous and no reliable K_d values could be extracted. C-lobe has been reported to dimerize through domain swapping.[15b] Yet it is unknown whether this dimerization mode contributes to the observed aggregation and viscosity. The aggregation of C-lobe also hampered reliable measurements of the circular dichroism (CD) spectrum of **10** to examine any handedness preference of the foldamer segment in the complex. Yet in the absence of C-lobe, the ^{1}H NMR spectrum of **10** exhibited characteristics of a helically folded foldamer component, such as deshielding of main chain amide protons involved in intramolecular hydrogen bonding (Figure S9).[12] Its CD spectrum showed a weak positive band indicating a slight bias in favor of *P* helicity (Figure S9). Note that the weak handedness bias is not in conflict with a well-folded aromatic helix. In other PQPQ–peptide macrocycles, strong handedness bias was observed with shorter peptide loops.[9a,12]

We next deciphered the interactions between **10** and C-lobe. The complex was successfully crystallized and its structure in the solid state was solved in space group *C*2 at 2.3 Å resolution (Figures S10–S17). The asymmetric unit contains two molecules of **10** and four of C-lobe. The protein has the same structure as the C-lobe of an intact E6AP HECT domain whose coordinates were used for molecular replacement (Figure 3b, PDB #1C4Z).[15a] The four proteins are in fact two disulfide-bridged dimers (Figures S11 and S13). Oxidation of Cys820 presumably occurred during crystallization. Yet this dimerization is unrelated to the domain swapping dimerization mentioned above[15b] as it does not alter the native C-lobe fold. The macrocycle **10** was found in a remarkable conformation in which both the peptide and foldamer segments are helically folded (Figure 3a, Figure S14), as if stapling each other. The peptide forms a slightly distorted α-helix, for example, with some bifurcated hydrogen bonds (Figure S15). With only eight residues involved (WRYVYQKC), the peptide helix would not be expected to be stable without an intramolecular staple.[20] The PQPQ helix matches well with earlier structures.[9a,12] It is exclusively *P* in the solid state. Crystal packing is relatively tight. As shown in detail in the Supporting Information, each macrocycle **10** makes contacts with four distinct proteins (Figures S10–S13, S16 and S17). However, most of the peptide residues that converged during display selection, that is, the α-helix, form an extended and intimate binding area with one of these four proteins (Figure 3b, c), whereas other contacts are limited and mostly concern the peptide residues that were not selected and one Q unit of the foldamer. It can therefore be inferred that the largest contact area—*ca.* 400 Å^2—constitutes the actual binding region. The proximity between the binding region and the disulfide bridge makes it impossible for two macrocycles to simultaneously bind a C-lobe disulfide dimer (Figure S13), shedding light on the 2:1 C-lobe-macrocycle stoichiometry in the crystal.

The protein–macrocycle interface of the complex involves extended hydrophobic contacts (with Gly755, Gly756, Ala805, Ile 803, Phe821, Val823), salt bridges, and hydrogen bonds (Figure S16). Several of the highly converged peptide residues show high shape and interaction complementarity with the protein surface, notably Trp7, Arg8, Tyr9, Val10 and Lys13 (Figure 3d–g). The most converged residue, Arg8, is clamped by Asp754 and Glu752 of C-lobe. Val10 occupies the core of the macrocycle and is in contact with both C-lobe and the foldamer. Altogether, the high convergence of the selection is largely explained by the involvement of the converged residues into a well-defined α-helical fold that forms extended, tight, and shape-complementary contacts with the selection target. As the only exception, Tyr11 displays high selection convergence yet it points away from the cognate C-lobe in the crystal structure.

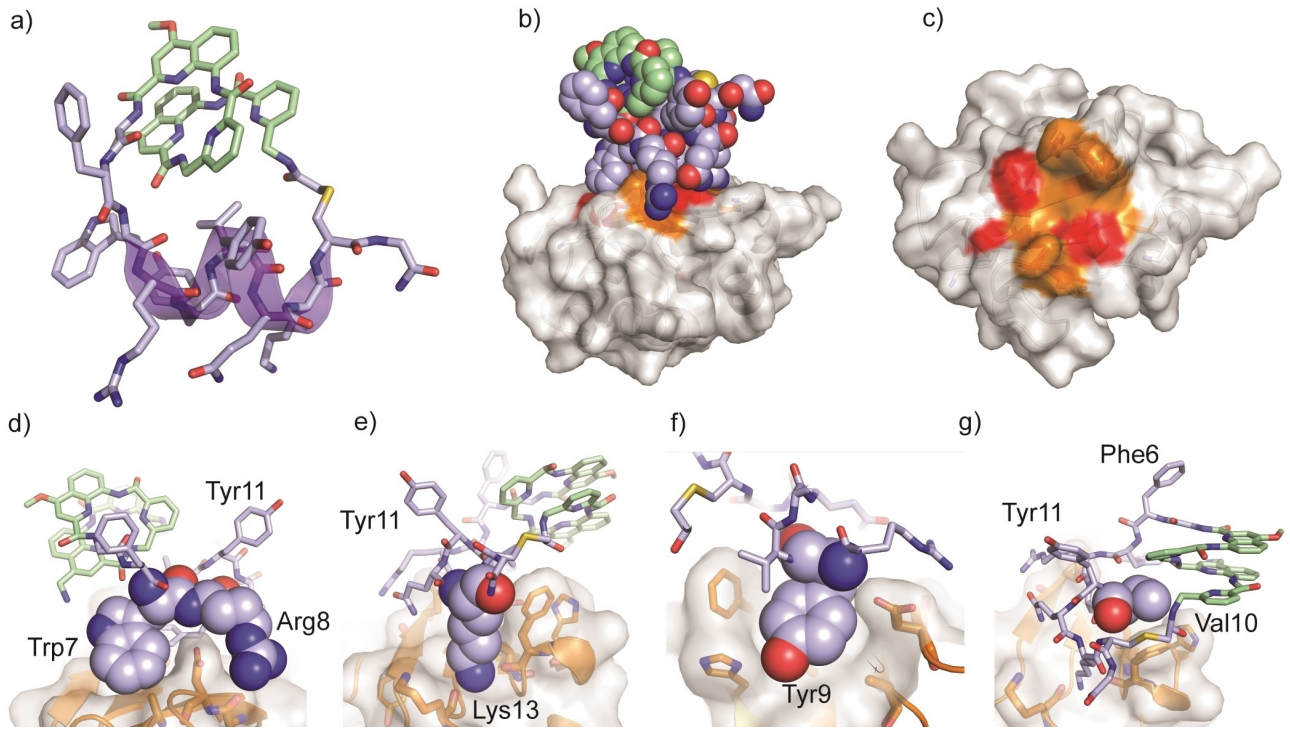

Figure 3. Crystal structure of the complex between C-lobe and macrocycle **10** (PDB #7QPB). a) View of the macrocycle alone showing the peptide and foldamer helices. b) Overall view of the complex. Macrocycle **10** is shown in space filling representation. c) Top view of the macrocycle binding site on the protein. Hydrogen bonds, salt bridges, and hydrophobic contacts are highlighted in orange, and longer distance hydrophobic contacts are shown in red. d–g) Specific macrocycle–protein contacts. Residues of interest are shown in space filling representation. Residues of **10** are numbered starting from the N-terminus of the foldamer segment (P1, Q2, P3, Q4, Gly5, Phe6 ..., Cys14, Gly15). Carbon atoms in green belong to the foldamer.

We then carried out an alanine scanning of the peptide α-helix. Macrocycles **11–17** were synthesized and their K_d values were measured by SPR. (Figure S8). Alanine is helicogenic and was not expected to destabilize the helix. Nevertheless, all Ala mutants showed weaker binding. For instance, the binding affinity collapsed for **11** (W7A) and **12** (R8A), was ten times lower for **17** and more than four times smaller for **13** (Y9A) and **16** (Q12A), consistent with the involvement of these residues in the binding. The effect was smaller for **14** (V10A), but we note that this mutant was the sixth most abundant sequence after the selection (Figure S6). Of note, binding also collapsed for **15** (Y11A) although the role of Y11 is not obvious from the structure of the complex.

MD simulations were used to shed further light on the macrocycle–protein interactions (Figure 4, Figures S18–S25). The complex found in the solid state was used as a starting point of MD runs. The complex underwent little change for some time. Upon prolonged simulation, the main interactions could be disrupted and other configurations were observed. Some contacts of the foldamer to the hydrophobic protein area occurred while the α-helix was still folded but exposed to water (Figure 4d). Such configuration might play a role along the coordinates that lead to complex formation but their actual contribution to the thermodynamic and kinetic parameters of the complex remains to be established.

MD runs of a V10A mutant suggested a destabilization of the α-helix (Figure S25, Table S2). A model of the macrocycle with an *M* foldamer helix was also built (Figure 4a) and energy minimized in complex with C-lobe while keeping the α-helix essentially intact. MD runs showed that the complex was kept in place with the same key peptide–protein interactions observed in the solid state for at least as long as with the *P* helix. The macrocycle with the *M* helix then also explored alternate configurations involving foldamer–protein contacts (Figure 4c). A notable feature was the tight and persistent stacking of Tyr11 on the *M* foldamer helix at the core of the macrocycle (Figures 4b and S24), in a role similar to that of Val10 with the *P* foldamer helix. Conversely, with the *M* foldamer helix, the V10A mutation did not result in a collapse of the α-helix (Figure S25, Table S2). These results suggest that Tyr11 and Val10 may act as macrocycle conformation stabilizers through foldamer–peptide contacts. Val10 may help stabilize the *P*-helical foldamer conformation whereas Tyr11 would stabilize the *M*-helical foldamer. As mentioned above, these hypotheses could not be verified experimentally due to protein aggregation. Further investigations of the exact role of each selected amino acid were deemed unessential at this stage and were not pursued.

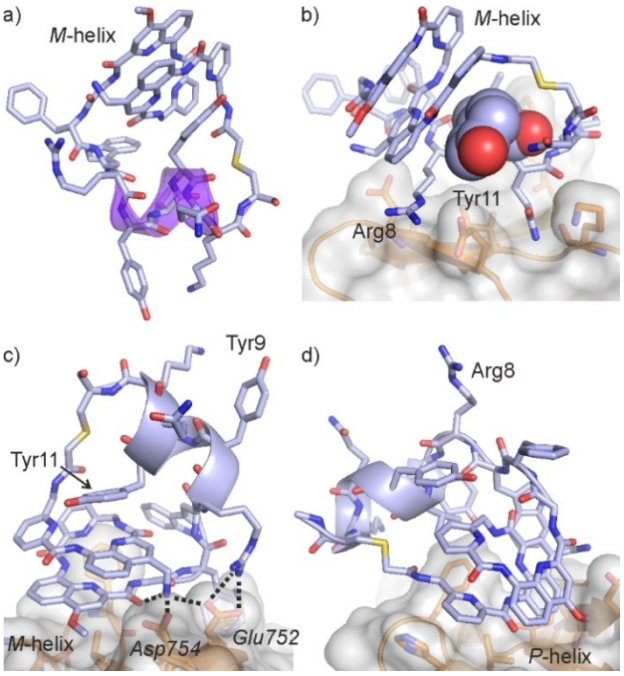

Figure 4. Snapshots of MD simulations of **10** in complex with C-lobe. a) View of *M*-helical **10** (the protein has been removed for clarity). b) Binding of *M*-helical **10** C-lobe in a mode similar to that of the crystal structure. c) Alternate arrangement found along the trajectory showing protein–foldamer contacts. d) Same as c) but with *P*-helical **10**. The α-helix of **10** is shown as a solid ribbon in (a), (c) and (d). Some hydrogen bonds are shown as dashed lines.

In summary, we have presented the first successful display selection of a macrocyclic peptide containing a large aromatic helical foldamer segment against a protein target. Selection was made possible by the sufficient yields of tRNA acylation and expression, despite the size—equivalent to a decapeptide—of the foldamer-containing initiator unit. Display selection showed high convergence toward a short and tight-binding peptide. Structural studies revealed a conformation in which both the peptide and foldamer are helical, as if stapling each other. The stapling of an α-helix by a foldamer helix is a new concept that will deserve further investigation to assess its potential general applicability. In the conformation bound to C-lobe, the foldamer helix protrudes as a large and rigid handle that may be modified to further enhance function, for example, to promote further contacts with the protein or to improve bioavailability. A key advantage of the aromatic foldamer unit would then be that it can be decorated with various substituents without altering its shape or the shape and function of the peptide residues. Research along these lines is currently being conducted and will be reported in due course.

Supporting Information

The authors have cited additional references within the Supporting Information.[22–41]

Acknowledgements

This work was supported by the Deutsche Forschungsgemeinschaft (DFG) through project HU1766/2-1 and CRC1309-C7 (project ID 325871075) to I. H. and by the JSPS Grant-in-Aid for Specially Promoted Research through project JP21H05618 to H. S. We thank Daniel Gill

and Binhao Teng for contributing some building block precursors. We thank I. Alonso for his help in the production of the alanine scanning macrocycles, S. Kwon for assistance with chemical synthesis and S. Lorenz for providing the expression vector for C-lobe. We are grateful to the European Synchrotron Radiation Facility (ESRF, Grenoble, France) for providing the beamtime (proposal mx2279), and Local Contact at the ESRF for providing assistance in using beamline ID23-1.[21] We thank University of the Sciences and West Pharmaceutical Services, Inc. for providing computational resources used for MD simulations Open Access funding enabled and organized by Projekt DEAL.

Conflict of Interest

The authors declare no conflict of interest.

Data Availability Statement

The data that support the findings of this study are available in the supplementary material of this article.

Keywords: Display Selection · Foldamers · Macrocycles · Peptides · Protein Recognition

[1] R. Barderas, E. Benito-Peña, *Anal. Bioanal. Chem.* **2019**, *411*, 2475–2479.
[2] J. A. Bernstein, M. Qazi, *Expert Rev. Clin. Immunol.* **2010**, *6*, 29–39.
[3] G. Molineux, A. Newland, *Br. J. Haematol.* **2010**, *150*, 9–20.
[4] M. Muttenthaler, G. F. King, D. J. Adams, P. F. Alewood, *Nat. Rev. Drug Discovery* **2021**, *20*, 309–325.
[5] a) Y. V. Guillen Schlippe, M. C. Hartman, K. Josephson, J. W. Szostak, *J. Am. Chem. Soc.* **2012**, *134*, 10469–10477; b) S. Imanishi, T. Katoh, Y. Yin, M. Yamada, M. Kawai, H. Suga, *J. Am. Chem. Soc.* **2021**, *143*, 5680–5684; c) X.-D. Kong, J. Moriya, V. Carle, F. Pojer, L. A. Abriata, K. Deyle, C. Heinis, *Nat. Biomed. Eng.* **2020**, *4*, 560–571; d) C. Tsiamantas, M. E. Otero-Ramirez, H. Suga, in *Cyclic Peptide Design. Methods in Molecular Biology, Vol. 2001*, Humana, New York, **2019**, pp. 299–315.
[6] a) C. A. Rhodes, D. Pei, *Chem. Eur. J.* **2017**, *23*, 12690–12703; b) H. Tsutsumi, T. Kuroda, H. Kimura, Y. Goto, H. Suga, *Nat. Commun.* **2021**, *12*, 696; c) T. R. Oppewal, I. D. Jansen, J. Hekelaar, C. Mayer, *J. Am. Chem. Soc.* **2022**, *144*, 3644–3652; d) X. Zheng, Z. Li, W. Gao, X. Meng, X. Li, L. Y. P. Luk, Y. Zhao, Y. H. Tsai, C. Wu, *J. Am. Chem. Soc.* **2020**, *142*, 5097–5103:; e) M. Zeng, F. Haeffner, J. Gao, *Chem. Sci.* **2022**, *13*, 8349–8354.
[7] a) T. Katoh, H. Suga, *J. Am. Chem. Soc.* **2022**, *144*, 2069–2072; b) T. Katoh, K. Tajima, H. Suga, *Cell Chem. Biol.* **2017**, *24*, 46–54; c) T. Kawakami, H. Murakami, H. Suga, *Chem. Biol.* **2008**, *15*, 32–42.
[8] a) B. Oller-Salvia, J. W. Chin, *Angew. Chem. Int. Ed.* **2019**, *58*, 10844–10848; b) A. E. Owens, J. A. Iannuzzelli, Y. Gu, R. Fasan, *ACS Cent. Sci.* **2020**, *6*, 368–381; c) X. S. Wang, P.-H. C. Chen, J. T. Hampton, J. M. Tharp, C. A. Reed, S. K. Das, D.-S. Wang, H. S. Hayatshahi, Y. Shen, J. Liu, W. R. Liu, *Angew. Chem. Int. Ed.* **2019**, *58*, 15904–15909.
[9] a) J. M. Rogers, S. Kwon, S. J. Dawson, P. K. Mandal, H. Suga, I. Huc, *Nat. Chem.* **2018**, *10*, 405–412; b) C. Tsiamantas, S. Kwon, C. Douat, I. Huc, H. Suga, *Chem. Commun.* **2019**, *55*, 7366–7369.
[10] C. Tsiamantas, S. Kwon, J. M. Rogers, C. Douat, I. Huc, H. Suga, *Angew. Chem. Int. Ed.* **2020**, *59*, 4860–4864.
[11] a) B. Baptiste, C. Douat-Casassus, K. Laxmi-Reddy, F. Godde, I. Huc, *J. Org. Chem.* **2010**, *75*, 7175–7185; b) H. Jiang, J.-M. Léger, I. Huc, *J. Am. Chem. Soc.* **2003**, *125*, 3448–3449; c) M. Kudo, V. Maurizot, B. Kauffmann, A. Tanatani, I. Huc, *J. Am. Chem. Soc.* **2013**, *135*, 9628–9631.
[12] S. Dengler, P. K. Mandal, L. Allmendinger, C. Douat, I. Huc, *Chem. Sci.* **2021**, *12*, 11004–11012.
[13] a) V. Azzarito, J. A. Miles, J. Fisher, T. A. Edwards, S. L. Warriner, A. J. Wilson, *Chem. Sci.* **2015**, *6*, 2434–2443; b) Z. Hegedus, C. M. Grison, J. A. Miles, S. Rodriguez-Marin, S. L. Warriner, M. E. Webb, A. J. Wilson, *Chem. Sci.* **2019**, *10*, 3956–3962; c) M. Jewginski, T. Granier, B. Langlois d'Estaintot, L. Fischer, C. D. Mackereth, I. Huc, *J. Am. Chem. Soc.* **2017**, *139*, 2928–2931; d) S. Kumar, M. Birol, D. E. Schlamadinger, S. P. Wojcik, E. Rhoades, A. D. Miranker, *Nat. Commun.* **2016**, *7*, 11412; e) S. Kumar, A. D. Hamilton, *J. Am. Chem. Soc.* **2017**, *139*, 5744–5755; f) M. Vallade, M. Jewginski, L. Fischer, J. Buratto, K. Bathany, J.-M. Schmitter, M. Stupfel, F. Godde, C. D. Mackereth, I. Huc, *Bioconjugate Chem.* **2019**, *30*, 54–62; g) K. Ziach, C. Chollet, V. Parissi, P. Prabhakaran, M. Marchivie, V. Corvaglia, P. P. Bose, K. Laxmi-Reddy, F. Godde, J.-M. Schmitter, *Nat. Chem.* **2018**, *10*, 511–518; h) J. Ahmed, T. C. Fitch, C. M. Donnelly, J. A. Joseph, T. D. Ball, M. M. Bassil, A. Son, C. Zhang, A. Ledreux, S. Horowitz, Y. Qin, D. Paredes, S. Kumar, *Nat. Commun.* **2022**, *13*, 2273.
[14] T. Seedorf, A. Kirschning, D. Solga, *Chem. Eur. J.* **2021**, *27*, 7321–7339.
[15] a) L. Huang, E. Kinnucan, G. Wang, S. Beaudenon, P. M. Howley, J. M. Huibregtse, N. P. Pavletich, *Science* **1999**, *286*, 1321–1326; b) L. K. Ries, A. K. Liess, C. G. Feiler, D. E. Spratt, E. D. Lowe, S. Lorenz, *Protein Sci.* **2020**, *29*, 1550–1554.
[16] Y. Yamagishi, I. Shoji, S. Miyagawa, T. Kawakami, T. Katoh, Y. Goto, H. Suga, *Chem. Biol.* **2011**, *18*, 1562–1570.
[17] M. Vallade, P. Sai Reddy, L. Fischer, I. Huc, *Eur. J. Org. Chem.* **2018**, 5489–5498.
[18] In an oligoamide sequence, Q^{Hyd} exists exclusively as the enol tautomer which results in an enhanced acidity, as opposed to that of keto tautomers. See: A. Albert, J. N. Philipps, *J. Chem. Soc.* **1956**, 1294–1304.
[19] There is no defined threshold to establish that an amino-acylation yield is sufficient for display selection. In the case of an initiation unit, a low yield may result in a second start (translation from the second codon instead of the AUG codon). In the current case, the outcome would be non-cyclic peptides unlikely to outcompete the macrocycles produced by successful initiation with the foldamer, even if the latter are produced in low yield.
[20] R. S. Harrison, N. E. Shepherd, H. N. Hoang, G. Ruiz-Gómez, T. A. Hill, R. W. Driver, V. S. Desai, P. R. Young, G. Abbenante, D. P. Fairlie, *Proc. Natl. Acad. Sci. USA* **2010**, *107*, 11686–11691.
[21] D. Nurizzo, T. Mairs, M. Guijarro, V. Rey, J. Meyer, P. Fajardo, J. Chavanne, J.-C. Biasci, S. McSweeney, E. Mitchell, *J. Synchrotron Radiat.* **2006**, *13*, 227–238.
[22] A. C. Wallace, R. A. Laskowski, J. M. Thornton, *Protein Eng.* **1995**, *8*, 127–34.
[23] H. Murakami, A. Ohta, H. Ashigai, H. Suga, *Nat. Methods* **2006**, *3*, 357–359.
[24] Y. Goto, A. Ohta, Y. Sako, Y. Yamagishi, H. Murakami, H. Suga, *ACS Chem. Biol.* **2008**, *3*, 120–129.

[25] T. Katoh, I. Wohlgemuth, M. Nagano, M. V Rodnina, H. Suga, **2016**, https://doi.org/10.1038/ncomms11657.
[26] T. Katoh, Y. Iwane, H. Suga, *Nucleic Acids Res.* **2017**, *45*, 12601–12610.
[27] Y. Hayashi, J. Morimoto, H. Suga, *ACS Chem. Biol.* **2012**, *7*, 607–613.
[28] D. J. Ford, N. M. Duggan, S. E. Fry, J. Ripoll-Rozada, S. M. Agten, W. Liu, L. Corcilius, T. M. Hackeng, R. Van Oerle, H. M. H. Spronk, A. S. Ashhurst, V. Mini Sasi, J. A. Kaczmarski, C. J. Jackson, P. J. B. Pereira, T. Passioura, H. Suga, R. J. Payne, *J. Med. Chem.* **2021**, *64*, 7853–7876.
[29] P. Emsley, B. Lohkamp, W. G. Scott, K. Cowtan, *Acta Crystallogr. Sect. D* **2010**, *66*, 486–501.
[30] D. Liebschner, P. V. Afonine, M. L. Baker, G. Bunkóczi, V. B. Chen, T. I. Croll, B. Hintze, L.-W. Hung, S. Jain, A. J. McCoy, N. W. Moriarty, R. D. Oeffner, B. K. Poon, M. G. Prisant, R. J. Read, J. S. Richardson, D. C. Richardson, M. D. Sammito, O. V. Sobolev, D. H. Stockwell, T. C. Terwilliger, A. G. Urzhumtsev, L. L. Videau, C. J. Williams, P. D. Adams, *Acta Crystallogr. Sect. D* **2019**, *75*, 861–877.
[31] E. Potterton, P. Briggs, M. Turkenburg, E. Dodson, *Acta Crystallogr. Sect. D* **2003**, *59*, 1131–1137.
[32] I. Jarmoskaite, I. AlSadhan, P. P. Vaidyanathan, D. Herschlag, *eLife* **2020**, *9*, 1–34.
[33] Z. Liu, A. M. Abramyan, V. Pophristic, *New J. Chem.* **2015**, *39*, 3229–3240.
[34] D. A. Case, H. M. Aktulga, K. Belfon, I. Y. Ben-Shalom, S. R. Brozell, D. S. Cerutti, T. E. Cheatham III, V. W. D. Cruzeiro, T. A. Darden, R. E. Duke, G. Giambasu, M. K. Gilson, H. Gohlke, A. W. Goetz, R. Harris, S. Izadi, S. A. Iz-mailov, K. Kasavajhala, A. Kovalenko, R. Kransy, T. Kurtzman, T. S. Lee, S. LeGrand, P. Li, C. Lin, J. Liu, T. Luchko, R. Luo, V. Man, K. M. Merz, Y. Miao, O. Mikhailovskii, G. Monard, H. Nguyen, A. Onufriev, F. Pan, S. Pantano, R. Qi, D. R. Roe, A. Roitberg, C. Sagui, S. Schott-Verdugo, J. Shen, C. L. Simmerling, N. R. Skrynnikov, J. Smith, J. Swails, R. C. Walker, J. Wang, L. Wilson, R. M. Wolf, X. Wu, Y. Xiong, Y. Xue, D. M. York, P. A. Kollman (2020), AMBER 2020, University of California, San Francisco.
[35] J. A. Maier, C. Martinez, K. Kasavajhala, L. Wickstrom, K. E. Hauser, C. Simmerling, *J. Chem. Theory Comput.* **2015**, *11*, 3696–3713.
[36] J. Wang, R. M. Wolf, J. W. Caldwell, P. A. Kollman, D. A. Case, *J. Comput. Chem.* **2004**, *25*, 1157–1174.
[37] J. Wang, P. Cieplak, P. A. Kollman, *J. Comput. Chem.* **2000**, *21*, 1049–1074.
[38] W. Kabsch, C. Sander, *Biopolymers* **1983**, *22*, 2577–2637.
[39] J. Buratto, C. Colombo, M. Stupfel, S. J. Dawson, C. Dolain, B. Langlois d'Estaintot, L. Fischer, T. Granier, M. Laguerre, B. Gallois, I. Huc, *Angew. Chem. Int. Ed.* **2014**, *53*, 883–887.
[40] S. De, B. Chi, T. Granier, T. Qi, V. Maurizot, I. Huc, *Nat. Chem.* **2018**, *10*, 51–57.
[41] V. Corvaglia, F. Sanchez, F. S. Menke, C. Douat, I. Huc, *Chem. Eur. J.* **2023**, e202300898.

Manuscript received: June 14, 2023
Accepted manuscript online: September 14, 2023
Version of record online: October 13, 2023